Sea level projections for South Asia

Supporting materials and methods

Benjamin Harrison - benjamin.harrison@metoffice.gov.uk

Reviewed by Joseph Daron and Matthew Palmer

August 2020

Contents

A1 Data

In this section we describe the methods and data sources used to generate the new South Asia regional sea level projections. The sea level projections for South Asia tide gauge locations are directly traceable to the process based global mean sea level (GMSL) projections presented the Fifth Assessment Report of the Intergovernmental Panel on Climate Change. Following Palmer et al. (2020), regional sea level projections are obtained by accounting for spatial patterns of sea level change from contributions to barystatic GMSL change (global ocean mass changes) and for relationships between local changes in ocean dynamic sea level with thermosteric GMSL change (global ocean density changes). We also account for spatial patterns of sea level changes from ongoing glacial isostatic adjustment (GIA, also referred to "post-glacial rebound").

A1.1 Tide gauge records

The regional sea level projections presented in this report are generated for tide gauge locations on the Indian Ocean and Arabian Sea coasts. Station data is sourced from the Permanent Service for Mean Sea Level (PSMSL, Holgate et al., 2012) .The latitude and longitude coordinates for Arabian Sea, Bay of Bengal and equatorial Indian Ocean are listed in tables A1.1a, A1.1b and A1.1c respectively. The records have not been corrected for vertical land motion, since projections include vertical land motion contributions associated with GIA and we do not want to remove the signal from the records. There are only a limited number of long duration (>50 years) tide gauge records available from the PSMSL for the South Asia region (indicated by colours in figures A1.1a-c. Many of the records contain gaps in data coverage (figure A1.2).

Figure A1.1a: *Location of the 18 tide gauge stations for Arabian Sea. Time series length of more than: 100 years (white), 75 years (yellow), 50 years (orange), more 30 years (brown). Less than 30 years (black). Adapted from https://www.psmsl.org, Data Explorer.*

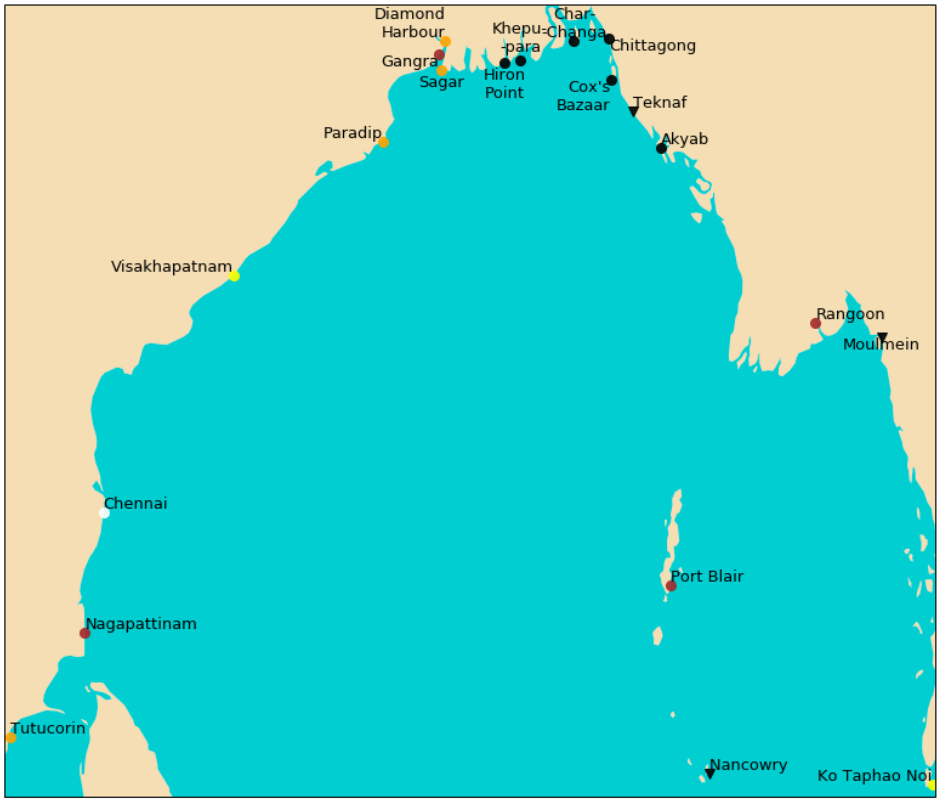

Figure A1.1b: *Locations for 20 of the 22 tide gauge stations for the Bay of Bengal. Time series length of more than: 100 years (white), 75 years (yellow), 50 years (orange), more 30 years (brown). Less than 30 years (black). Adapted from https://www.psmsl.org, Data Explorer.*

Figure A1.1c: *Location of the 11 tide gauge stations for the Equatorial Indian Ocean. Time series length of more than: 100 years (white), 75 years (yellow), 50 years (orange), more 30 years (brown). Less than 30 years (black). Adapted from https://www.psmsl.org, Data Explorer.*

Tide gauge	Latitude	Longitude	Nation	Dataset
Djibouti	11.608	43.139	Djibouti	PSMSL (metric)
Bhaunagar	21.75	72.233	India	PSMSL
Mangalore	23.628	58.565	India	PSMSL
Veraval	20.9	70.367	India	PSMSL
Kandla	23.017	70.217	India	PSMSL
Okha	22.467	69.083	India	PSMSL
Mormugao	15.417	73.8	India	PSMSL
Vanidar	22.45	69.833	India	PSMSL
Cochin	9.967	76.267	India	PSMSL
Mumbai	18.917	72.833	India	PSMSL
Chabahar	25.295	60.603	Iran	PSMSL
Salalah	16.933	54	Oman	PSMSL
Masriah	20.217	58.483	Oman	PSMSL
Muscat	12.917	74.8	Oman	PSMSL
Ormara	25.2	64.067	Pakistan	UHSLC
Gwadar Port	25.117	62.333	Pakistan	PSMSL (metric)
Karachi	24.812	66.975	Pakistan	PSMSL
Aden	12.788	44.974	Yemen	PSMSL

***Table A1.1a**: Details for the 18 tide gauge stations from the Arabian Sea. Stations without benchmarked tide-gauge station records are referred to as "metric" stations on PSMSL as indicated by the "Dataset" column. Ormara tide gauge data taken from the University of Hawaii Sea level Center (UHSLC).*

Tide gauge	Latitude	Longitude	Nation	Dataset
Port Blair	11.683	92.767	Andaman Islands (Indian Union Territory)	PSMSL
Nancowry	08.050	93.550	Andaman Islands (Indian Union Territory)	PSMSL (metric)
Cox's Bazaar	21.450	91.833	Bangladesh	PSMSL
Hiron Point	21.783	89.467	Bangladesh	PSMSL
Khepupara	21.833	89.833	Bangladesh	PSMSL
Khal #10*	22.267	91.816	Bangladesh	PSMSL (metric)
Char Changa	22.216	91.050	Bangladesh	PSMSL
Chittagong	07.833	98.433	Bangladesh	PSMSL
Teknaf	20.833	92.300	Bangladesh	PSMSL (metric)
Nagapattinam	10.767	79.850	India	PSMSL
Diamond Harbour	22.200	88.167	India	PSMSL
Gangra	21.950	88.017	India	PSMSL
Tutucorin	08.750	78.200	India	PSMSL
Paradip	20.267	86.700	India	PSMSL
Haldia*	22.033	88.100	India	PSMSL
Visakhapatnam	17.683	83.283	India	PSMSL
Chennai	13.100	80.300	India	PSMSL
Sagar	21.650	88.050	India	PSMSL
Akyab	16.767	96.167	Myanmar	PSMSL
Rangoon	20.133	92.900	Myanmar	PSMSL
Moulmein	16.465	97.622	Myanmar	PSMSL (metric)
Ko Taphao Noi	22.247	91.825	Thailand	PSMSL

***Table A1.1b**: Details for the 22 tide gauge stations from the Bay of Bengal. Stations without benchmarked tide-gauge station records are referred to as "metric" stations on PSMSL as indicated by the "Dataset" column. The asterisk indicates locations not shown in figure A1.1b due to proximity to other stations.*

Tide gauge	Latitude	Longitude	Nation	Dataset
Diego Garcia	-0.683	75.15	British Overseas Territory	PSMSL
Padang	-7.29	72.393	Indonesia	PSMSL
Sibolga	5.888	95.317	Indonesia	PSMSL
Sabang	6.767	73.173	Indonesia	PSMSL
Minicoy	6.935	79.858	Lakshadweep (Indian Union Territory)	PSMSL (metric)
Hanimadhoo	-4.467	55.533	Maldives	PSMSL (metric)
Gan	-6.15	39.183	Maldives	PSMSL
Male	4.183	73.533	Maldives	PSMSL
Point La Rue	-0.967	100.375	Seychelles	PSMSL
Colombo	1.75	98.767	Sri-Lanka	PSMSL (metric)
Zanzibar	8.283	73.05	Tanzania	PSMSL

***Table A1.1c**: Details for the 11 tide gauge stations from equatorial Indian Ocean. Stations without benchmarked tide-gauge station records are referred to as "metric" stations on PSMSL as indicated by the "Dataset" column.*

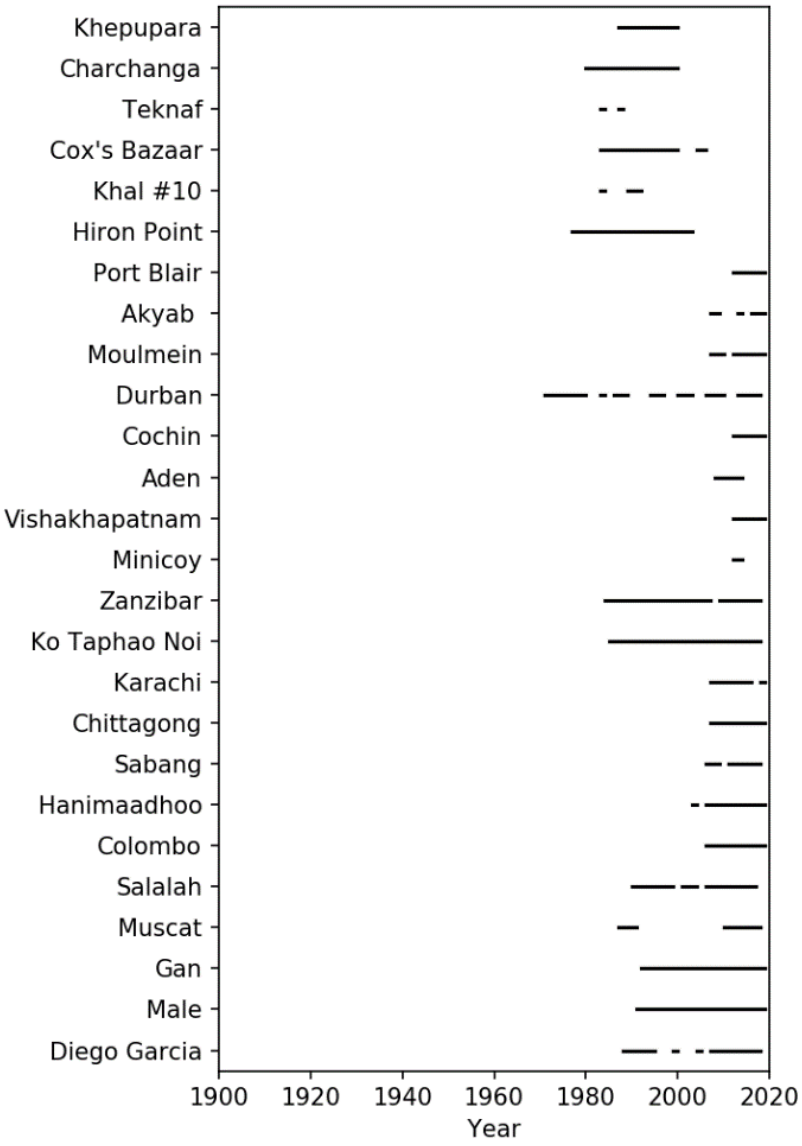

***Figure A1.2**: Data coverage for Indian Ocean tide gauge records based on data from the University of Hawaii Sea level centre (UHSLC).*

A1.2 Satellite Altimeter Data

Satellite altimeter data from v2.0 of the European Space Agency (ESA) Climate Change Initiative for observations of sea level[1] (Legeais et al., 2018) was obtained to supplement tide gauge observations. The ESA satellite altimetry dataset is based on gridded observations from nine altimeter missions from the period 1993-2015, that provided monthly mean values for GMSL on a 0.25-degree latitude-longitude grid. The gridded observations have been homogenized and reprocessed. The monthly-mean values for GMSL anomalies were converted to annual-mean values to allow for comparisons with the projections of GMSL. The ESA altimetry product also provides two dimensional fields such as gridded sea level anomalies. The monthly-mean gridded sea-level anomalies were converted to annual-mean anomalies to allow for comparisons with the regional sea level projections. For the tide gauge locations in this study (shown in figures A1.1a, A1.1b and A1.1c), an annual mean time series was selected the closest available grid box.

A1.3 Climate model data

The sea level projections presented in this report were generated using the methods developed for UKCP18, described in the UKCP18 Marine Projections report (Palmer et al., 2018a) and in Palmer et al. (2020). The sea level projections are generated from climate model simulations conducted for the Coupled Model Intercomparison Project Phase 5 (CMIP5). A full list of the CMIP5 models used in this study can be found in Church et al, 2013. The methods are an extension of those presented in the IPCC AR5, with updated and scenario-dependent projections of the contribution to GMSL change from dynamic ice processes in Antarctica based on (Levermann et al., 2014). Over the 21st century, these methods provide very similar projections to the recently published IPCC SROCC (Oppenheimer & Glavovic, 2019).

The 21st century sea level projections for South Asian tide gauge locations are based on the same 21-member Global Circulation Model (GCM) ensemble from CMIP5 used for GMSL projections in the IPCC AR5 (Church et al., 2013). The projections use simulations of global-mean surface temperature and global-mean thermosteric sea level rise under different greenhouse gas representation concentration pathway (RCP) scenarios.

The sea level projections also include simulations of ocean dynamic sea level change from the CMIP5 ensemble, which arise from local variations in ocean density and ocean circulation. Simulated changes in local ocean dynamic and global thermosteric sea level are combined to determine the contribution to sea level change from ocean processes. In this report these sea level changes are referred to collectively as sterodynamic sea level change, following (Gregory et al., 2019). Following previous studies (Cannaby et al., 2016; Gupta et al., 2013; Palmer et al., 2018a; Palmer et al., 2020), sea level data are drift-corrected for each CMIP5 model based on a linear fit between the forced climate simulation and the pre-industrial control simulation. At each tide gauge location regression relationships are established between sterodynamic

[1] Note: European Space Agency satellite altimetry: http://www.esa-sealevel-cci.org/ .

sea level change and global thermosteric sea-level change for each CMIP5 model. For more details, see the methods section of the UKCP18 Marine Report (Palmer et al., 2018a)

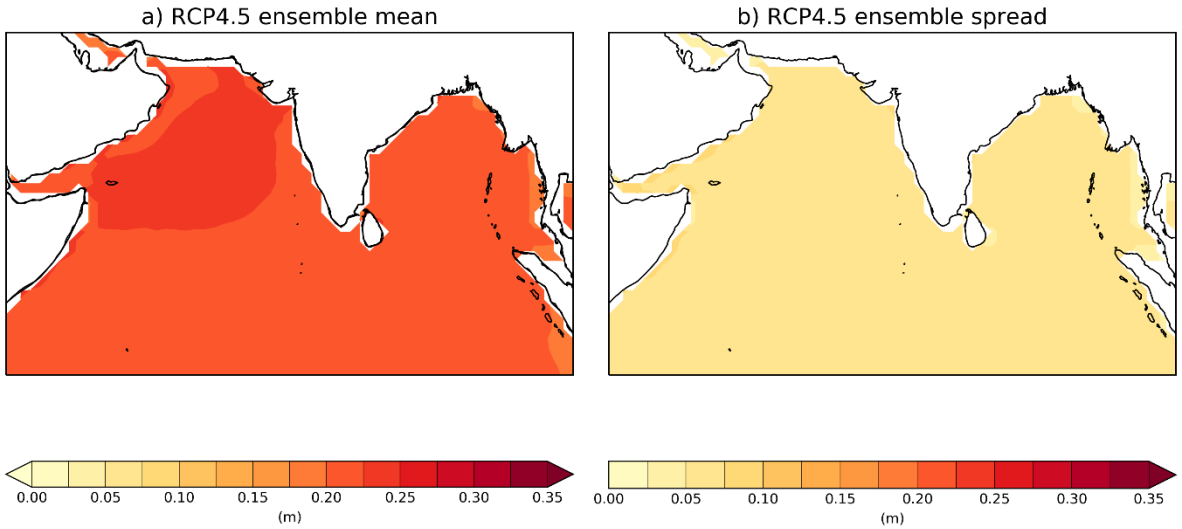

***Figure A1.3**: Projections of time averaged sterodynamic (steric and dynamic) sea level changes for the period 2081-2100 relative to the baseline period of 1986-2005 from 21 CMIP5 models under RCP4.5. Left panel shows the ensemble mean and right panel shows the ensemble spread based on the 90% confidence interval of the standard deviation. The spatial patterns arise from forced response of ocean dynamic sea level across the 21 CMIP5 models in the ensemble. Reproduced from SROCC (Oppenheimer et al. 2019).*

Spatial patterns for sterodynamic sea level changes under RCP4.5 are shown in figure A1.3. The spatial pattern of the multi-model response to sterodynamic change shows an increase in the sea level gradient across the Southern Ocean, with an associated increase in sea level over the Arctic and North Atlantic Oceans. By contrast the sterodynamic contribution to sea level changes over the Arabian Sea and Bay of Bengal are more spatially homogeneous. Similarly, multi-model spread in sterodynamic sea level change is larger over Arctic and North Atlantic Oceans, than for the corresponding spread in sterodynamic sea level change over the Arabian Sea and Bay of Bengal. The relative spatial homogeneity in sterodynamic sea level changes and model over the Arabian Sea and Bay of Bengal is not a general feature of tropical basins, since large sea level gradients can be seen the tropical Pacific and tropical Atlantic.

The sea level height over the Bay of Bengal, Arabian sea and Equatorial Indian Ocean regions are influenced by variations in ocean density and ocean circulation. Local sea levels are partly determined by changes to ocean dynamic sea level. In order to account for the sterodynamic contribution, we compare the ocean dynamic sea level and global-mean thermosteric sea level in each of the 21 CMIP5 models, under the RCP2.6, RCP4.5 and RCP8.5. For each model in the ensemble, we establish a regression relationship between the local sterodynamic sea level change and global-mean thermosteric sea level change at each tide gauge location.

A1.3 Gravitation, Rotation and Deformation patterns

The redistribution of water and ice mass from the land to the ocean results in geographically dependent changes to mean sea level (MSL). The spatial variations in MSL change arise due to the changes in the gravitational field, changes in the contribution to geopotential from Earth's rotation and deformation of the Earth's surface (Mitrovica et al., 2001). Following (Gregory et al., 2019), we refer to these changes collectively as GRD (Gravity, Rotation, Deformation) but the term mass fingerprints can also be used (as in UKCP18).

As with the UKCP18 sea level projections we use two estimates of the GRD patterns for the different ice mass terms, provided by Spada and Stocchi (2007) and Slangen et al. (2014). A single estimate is used for the contribution from changes to land water storage – arising through groundwater extraction and reservoir impoundment – based on projections provided by Wada et al. (2012). The land water contribution to MSL changes is partly based on estimates of changes to water demand. The magnitude and spatial variation of the land water contribution is projected to be larger for the basins in the South Asia region compared to other regions, due to the large population density and expected increase in water demand with rising population. The sea level projections presented in this report account for some of the uncertainty from different GRD models but do not account for contributions to uncertainty in the geographic distribution of mass change. However, Palmer et al. (2020), found that the uncertainty associated with the choice the GRD estimates to be negligible and the same set of GRD solutions were used in this study.

The spatial patterns in figure A1.4 show estimated contributions from GRD to local MSL change. The values can be thought of as scaling factors representing the local change in MSL per unit rise in GMSL. GRD estimates are provided for contributions from: (a) Antarctic surface mass balance; (b) Antarctic ice dynamics; (c) Glaciers; (d) Greenland surface mass balance; (e) Greenland ice dynamics; (f) changes in land water storage. The contributions arising from the loss of ice stored in the Antarctic and Greenland ice sheets are characterised by fall in MSL near the ice sheets and an increased rise in MSL away from the ice sheets (i.e. greater than unity increase relative to GMSL rise).

Over the South Asia region, the Greenland GRD patterns are spatially homogeneous, except for the far north of the Arabian sea. In contrast the spatial patterns for the corresponding contributions from Antarctica show a more zonally asymmetric contribution from ice dynamics compared to surface mass balance. The zonal asymmetry in the Antarctica ice dynamics contribution manifests as an equatorward extension of the zero-line contour from the West Antarctic Ice Sheet, the region of projected ice mass loss. The zero-line contour represents the transition from the near-field fall in local MSL and far-field rise in local MSL relative to GMSL rise. A corresponding poleward extension south of the Indian sub-continent is indicated by the trough in zero-line contour, with the trough axis oriented approximately north-south through the centre of the Indian sub-continent. This roughly coincides with the meridian

separating the Arabian Sea and Bay of Bengal regions in this study, which lie respectively to the east and west of the trough axis.

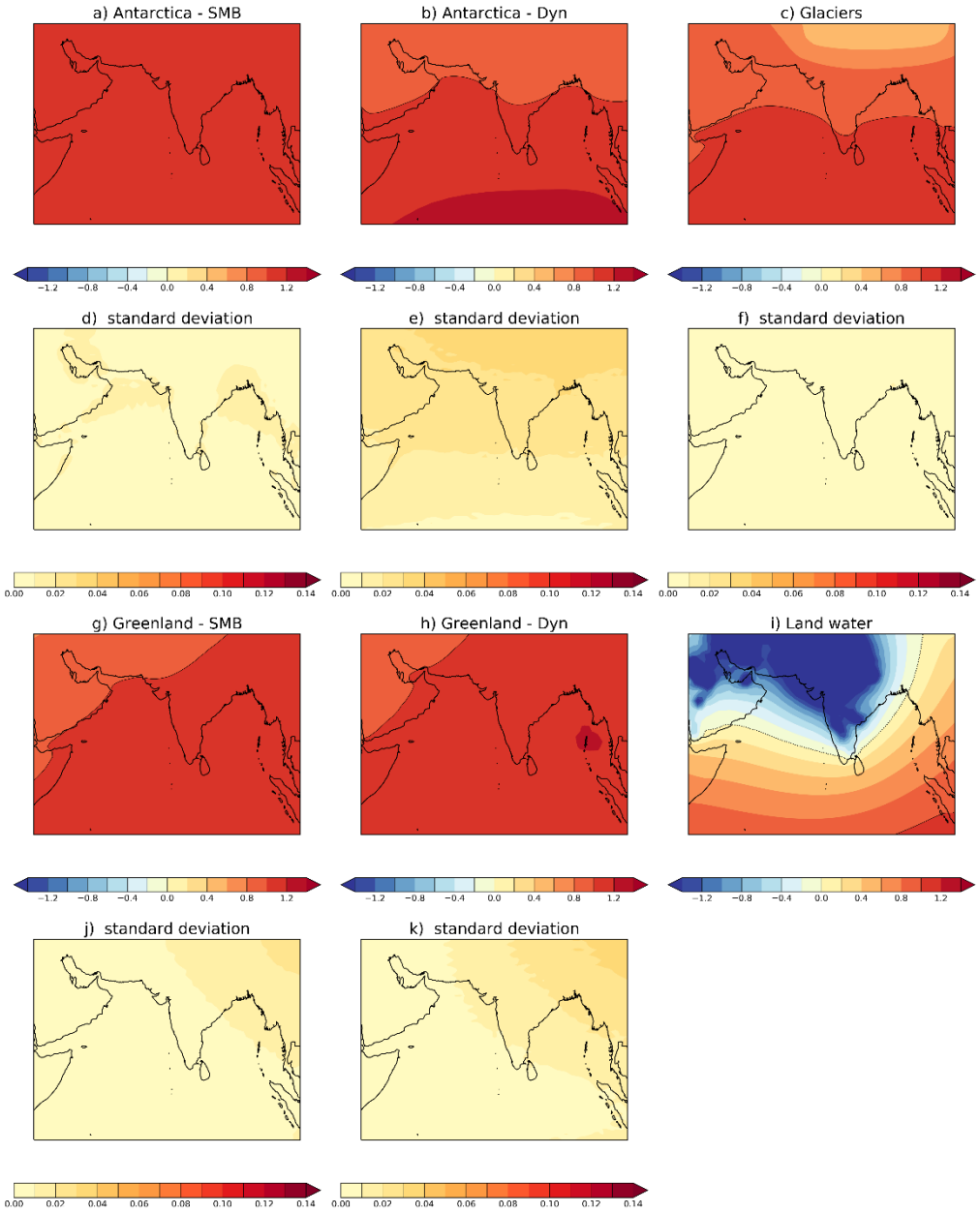

***Figure A1.4**: Spatial patterns representing the effect of mass changes on the fields associated with the Earth's Gravity (G) and Rotation (R), along with differences in the Deformation of the solid-earth surface (D). The spatial patterns show the combined effect of GRD on local mean sea level for each GMSL component, expressed as local mean sea level change per metre of global mean sea level change. The zero contour, corresponding to no-change in local MSL is indicated by the dotted line. The unit-contour, corresponding to identical local MSL and GMSL change is indicated by the solid line. Panels a,b,c, g, h and i show the mean across different GRD model estimates ,with panels d,e,f,j and k showing the corresponding standard deviations across the GRD models*

The spatial patterns for the GRD contributions from glaciers are spatially more complex, due to the non-uniform distribution of the world's glaciers (i.e. highly localised areas of glacier ice over high altitude regions). For most of tide gauge locations

selected in this study the contribution to local MSL change relative to GMSL rise is less than unity. For the Bay of Bengal, tide gauge locations approximately south of (and including) Chennai lie in the region with a greater than unity contribution from glacier mass to local MSL relative to GMSL. The corresponding region for the Arabian sea covers tide gauge locations south of (and including) Cochin. The spatial patterns from GRD can have a significant impact on projections of regional and local MSL changes. For the South Asia region, the land water storage component changes sign over Arabian Sea and Bay of Bengal, contributing to sea level rise in some areas and reducing sea level rise in others.

Across the GRD estimates the spatial patterns in standard deviation reveal that the largest differences are seen in the regions with the largest mass change, namely around the ice sheets and high latitude glaciers. The standard deviation could not be computed for the GRD pattern for land water storage, because the GRD estimate for the land water storage contribution was based on a single model solution. Since Palmer et al. (2020) found the negligible uncertainty for the choice of GRD estimates, therefore we assume the same is true for the GRD patterns arising from the land water barystatic component. While the uncertainty associated with the patterns of spatial change are assumed to be low for land water storage, the same is not true for the magnitude of change. The land water contribution to global sea level rise assumes that 100% of extracted groundwater is transferred to the oceans, which more recent studies suggest the figure is closer to 80% (Wada et al. 2014). However, the revised estimate would not modify the spatial pattern of change, since the GRD pattern depends on the locations of mass change, as discussed for ice sheet patterns.

A1.4 Glacial isostatic adjustment

The sea level projections presented in this report include estimates for the contribution of Glacial Isostatic Adjustment (GIA) to local MSL change. GIA refers to the adjustment of the Earth's lithosphere and underlying viscous mantle towards hydrostatic equilibrium in response to the transfer of ice mass to oceans since the last glaciation (Tamisea and Mitrovica 2011). Since adjustment process takes place over thousands of years (i.e. the response since the last glaciation), the rate of adjustment is treated as approximately constant for the multi-decadal and centennial sea level projections in this report. This redistribution of mass from land to the oceans, also alters the Earth's geopotential energy field due to gravitational and centrifugal changes.

For some areas, GIA can contribute to important meridional differences in MSL change, as seen for sea level projections for tide gauge locations in the UK (Palmer et al. 2018a, Howard et al. 2019) and locations in Scandinavia (Palmer et al. 2020). In contrast, the spatial patterns for GIA over the tropics feature less spatial heterogeneity and much smaller contributions to local MSL change, compared to high latitudes. For the South Asia region, the contributions from GIA to overall sea level rise are generally insignificant but the spatial variations (figure A1.4) in GIA do contributes to differences in sea level change between locations.

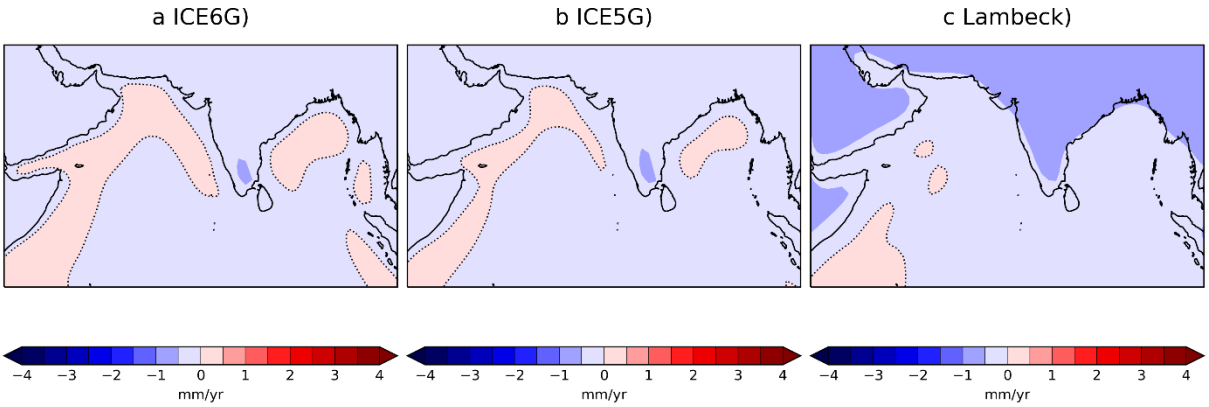

***Figure A1.4**. a)-c) Three estimates for the effect of glacial isostatic adjustment (GIA) on sea level change. The zero line is indicated by the dotted contours.*

Following Palmer et al. 2020, three global GIA estimates were used for the sea level projections presented in this report. The estimates were based on the ICE-5G model (Peltier, 2004), ICE-6G model (Argus et al., 2014; Peltier et al., 2015) and an independent estimate from the Australian National University based on an update of Nakada and Lambeck (1988). For the South Asia region, the ICE-5G and ICE-6G estimates show small differences in the position of the zero-line contour, which is slightly further away from the Indian sub-continent land mass in the ICE-6G. In the Lambeck GIA estimate, the contribute to sea level change is zero over much of the South Asia region. The standard deviation from the three GIA estimates over the South Asia region suggests these differences are not significant (not shown, see Palmer et al., 2020).

A2 Methods

A2.1 Global sea level projections

The MSL projections for the South Asia tide gauge locations discussed in this report are based on the process-based projections of GMSL presented in IPCC AR5 (Church et al. 2013) for the period 2007-2100. The GMSL projections include estimates for the contribution to GMSL from (i) global-mean thermosteric sea level and six barystatic contributions to GMSL: (ii) Antarctica surface mass balance; (iii) Antarctic ice dynamics; (iv) Greenland surface mass balance (v); Greenland ice dynamics; (vi) Glaciers; and (vii) land water storage changes (see table A2.1) The 21st century projections use simulations of global-mean thermosteric sea level and global mean surface change from 21 CMIP5 models under RCP2.6, RCP4.5 and RCP8.5. The 21 CMIP5 models are the same as those used for the IPCC AR5 GMSL projections.

The extended sea level projections for 2100-2300 follow the physical-emulator approach described in the UKCP18 Marine Projections report (Palmer et al. 2018b). The 2100-2300 projections are based on a GCM emulator tuned to reproduce simulations of 16 CMIP5 models using the extended RCP scenarios (Meinshausen et

al. 2011). The extended sea level projections use 11 of 21 CMIP5 models used for the 21st century sea level projections.

Component of Global Mean Sea Level	Method for 21st Century Projection estimates	Method for 2300 Projection estimates
(i) Global average thermosteric contribution (ocean thermal expansion)	Projections are based on the ensemble of 21 CMIP5 model simulations used for the global mean sea level projections in IPCC AR5 (Church et al. 2013)	Projections are based on an emulator on ensemble from 16 emulated CMIP5 models (Palmer et al. 2018) with expansion efficiencies documented by Lorbacher et al. (2015)
(ii) Antarctica - surface mass balance	Projections are based the relationship between global surface temperature change and Antarctic surface mass balance. The projections for global surface temperature change are provided by simulations from the 21 CMIP5 models used in global sea level projections for IPCC AR5 (Church et al. 2013)	The same relationship between surface mass balance and global surface temperature change is applied to 2300. Projections for global surface temperature change are produced from the 16-member ensemble of emulated CMIP5 models used in UKCP18 (Palmer et al. 2018a)
(iii) Antarctica – ice dynamics	Scenario-dependent statistical fit to results from Levermann et al. (2014), applied over the 21st century, as described in the UKCP18 Marine Projections (Palmer et al. 2018a and Palmer et al. 2020)	The 2100 rate is held constant between 2100 and 2300
(iv) Greenland – surface mass balance	Projections are based the relationship between global surface temperature change and Greenland surface mass balance. The projections for global surface temperature change are provided by simulations from the 21 CMIP5 models used in for global sea level projections in IPCC AR5 (Church et al. 2013)	The 2100 rate is held constant between 2100 and 2300
(v) Greenland – ice dynamics	Scenario-dependent estimate, based literature available for IPCC AR5 (Church et al. 2013)	The 2100 rate is held constant between 2100 and 2300
(vi) Glaciers	Projections are based on a relationship between global surface temperature change and worldwide glacier-mass loss, used for global sea level projections in IPCC AR5 (Church et al. 2013)	The same relationship between global temperature change and worldwide glacier mass loss is applied out to 2300 (Church et al. 2013), with the maximum contribution to global sea level rise capped at 0.32 m based on estimates of the remaining water volume stored in worldwide glaciers(Grinsted 2013, Farinotti et al. 2019). Projections for global surface temperature change are provided by the 16-member ensemble of emulated CMIP5 models (Palmer et al. 2018a).
(vii) Land Water Storage	Scenario dependent estimate based on literature available at the time of IPCC AR5	The 2100 rate is held constant between 21000 and 2300

Table A2.1: *The components of Global Mean Sea Level change, (left column). The methods used to determine the components for the 21st century projections (centre column) and extended range projections (right column).*

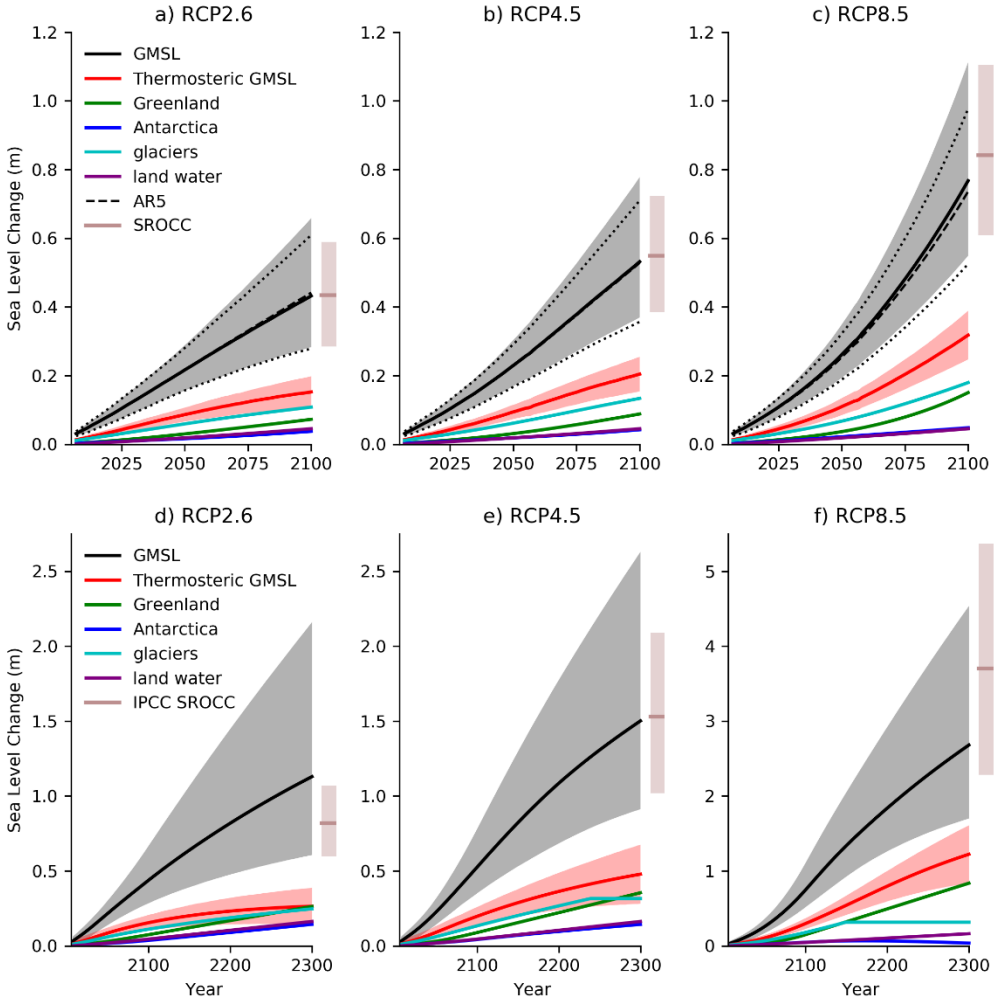

***Figure A2.1**: Global Mean Sea level projections under RCP2.6 (a), RCP4.5 (b) and RCP8.5 (c) over the 21st century. Extended Global Mean Sea level projections under the corresponding extended RCPs (d-f) for the period 2100-2300. The contributions from the different components of Global Mean Sea level are shown, as indicated by the legend. The shaded regions indicate 5th to 95th percentile range from the 450,000 member Monte Carlo simulations for the combined sea level change (grey) and the thermosteric component (red). The dotted lines show the 5th to 95th percentile range, while the dashed line shows the 50th percentile range from the Monte Carlo Simulations used for Global Mean Sea level projections presented in IPCC AR5 (Church et al. 2013). Projections are relative to the baseline period of 1986-2005.*

The projections described in this report use scenario-dependent estimates for the contribution of Antarctica ice dynamics described in the UKCP18 Marine Projections report based on parametrisations from Levermann et al. (2014). As with the UKCP18 Marine Projections, the estimate for the Antarctic ice dynamics component does not include the possibility of additional contributions from ice sheet instabilities in the West Antarctic Ice Sheet. For the West Antarctica ice sheet, the transfer of ice mass to the oceans is governed primarily by dynamic ice flow processes rather than surface mass balance (the net change due to snow accumulation and snow melt) that dominates over the East Antarctica ice sheet. Satellite studies and modelling studies have suggested there could be additional contributions to global sea level rise from the rapid collapse of the West Antarctica ice sheet, through positive feedback mechanisms know

as 'Marine Ice Sheet Instability' and 'Marine Ice Cliff Instability' (DeConto & Pollard, 2016)The latter describes the process where marine terminating ice shelves disintegrate leaving behind taller ice cliffs and these can be structurally unstable if taller than 100m. The disintegration of the structurally unstable ice cliffs, results in further unstable ice cliffs leading to self-sustaining ice losses, resulting in potentially large contributions to global sea level rise. Edwards et al. (2019) suggest the contribution to global sea level rise from marine ice cliff instability have been overestimated and updated estimates that include ice sheet instabilities result in a similar projected range to Levermann et al. (2014).

The South Asia sea level projections in this report follow the same approach as in the UKCP18 Marine Projections report (Palmer et al. 2018a) based on the Monte Carlo procedure used for the IPCC AR5 GMSL projections. The components of GMSL are combined using a 450,000-member ensemble which samples the underlying distributions. For scenario dependent contributions to GMSL these distributions are based on the 5th and 95th percentile ranges from the CMIP5 model simulations. The range for the scenario dependent land water storage component contribution to GMSL is based on the literature assessed for IPCC AR5. The Monte Carlo procedure preserves the correlations between global thermosteric sea level changes and global mean surface temperature changes within the CMIP5 model simulations. Since each member of the Monte Carlo ensemble generates time series for the seven components of GMSL, the variable correlations within the CMIP5 model simulations result in correlations between different components of the GMSL projections.

For the extended projections for 2100-2300 the ensemble spread arises from differences in the simulated variables across the emulated CMIP5 models. As with the 21st century projections the Monte Carlo ensemble procedure samples the distributions based on the 5th and 95th percentiles but from the set of 16 emulated CMIP5 models. In the extended projections, the contribution to sea level change from melting glaciers is limited by the total ice mass stored in worldwide glaciers. Based on current estimates of total glacier mass (Farinotti et al., 2019; Grinsted, 2013)the contribution from glacier mass to GMSL is capped at 0.32m. We make the simplifying assumption that all the remaining glacier ice mass is transferred to the oceans. This is does not account for the possibility of the glaciers reaching a new steady state following the preferential melting of low altitude glacier ice, leading to smaller contributions to sea level rise from worldwide glaciers.

A2.2 Regional sea level projections

The previous sub-section explained that GMSL projections were generated from estimates for seven physical processes that contribute to GMSL change. For the South Asia MSL projections, we must also account for the additional processes that contribute to MSL at the regional scale. These include estimates for the contribution to MSL arising from changes in ocean circulation and ocean density. In UKCP18 these contributions were referred to collectively as the oceanographic component, however

following (Gregory et al., 2019) we refer to these contributions as the sterodynamic component of MSL. This component is estimated by establishing regression relationships between global average thermosteric sea level change and the local sterodynamic sea level change at the tide gauge locations in each of the CMIP5 simulations. Figure A2.2, shows the regression relationship between local sea level at Karachi, Pakistan and global thermosteric sea level for the 21 CMIP5 models. The 1:1 relationship is shown for comparison.

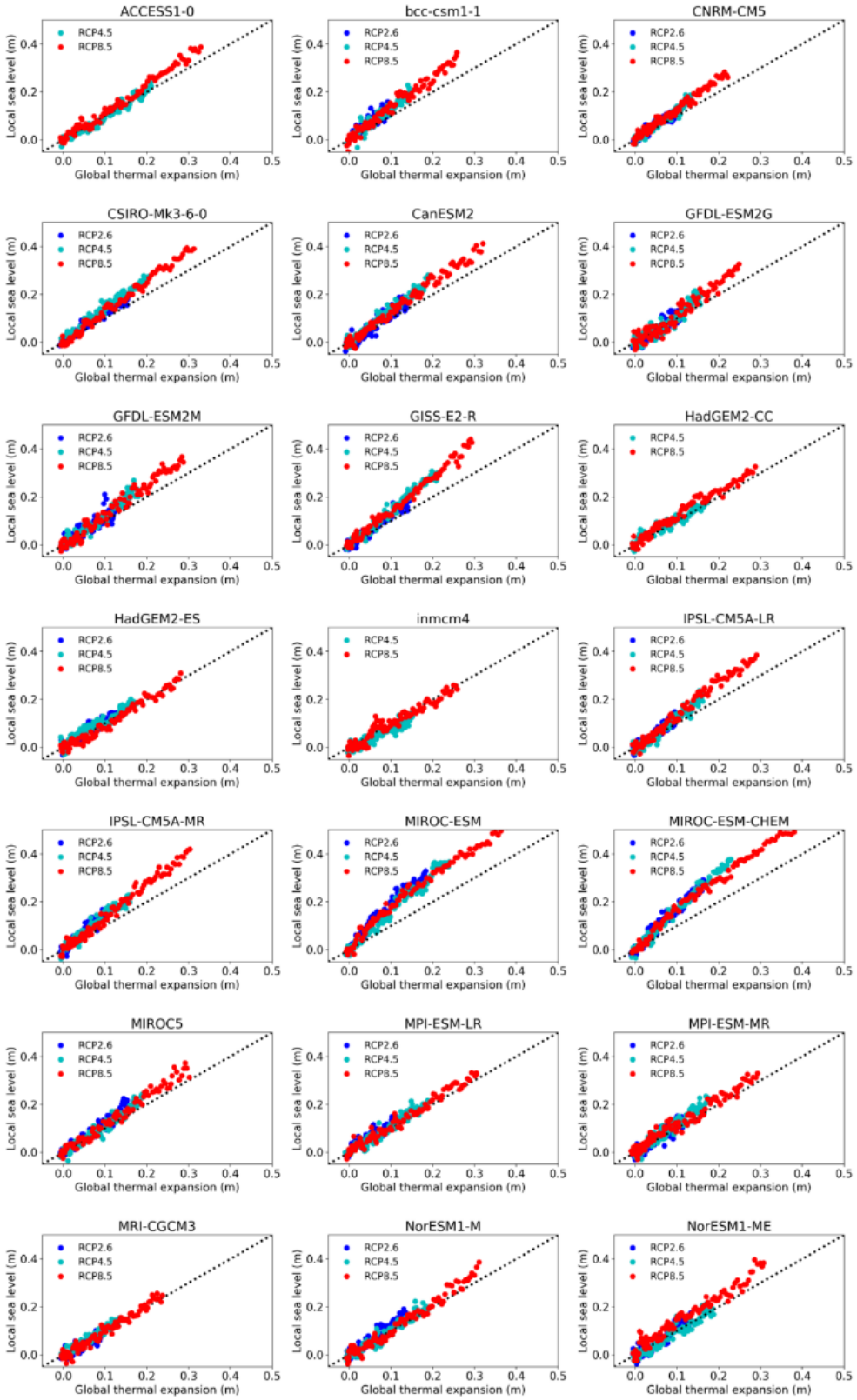

Figure A2.2: *Regression relationship between local sterodynamic sea level and global thermal expansion at Karachi for the period 2007-2100 from the 21 CMIP5 models. Relationships are determined for all available simulations: RCP2.6 (blue); RCP4.5 (cyan); and RCP8.5 (red). For comparison, the dotted line shows the 1:1 relationship.*

The barystatic components of GMSL are geographically dependent, with spatial variations that arise from the response of the Earth's gravitational-rotational field in response to the redistribution of mass and the deformation of the solid earth surface (GRD). The barystatic contribution to regional MSL is estimated using the different GRD models. Finally, we include estimates for the effect of VLM due to GIA on regional MSL. Figure A2.3 shows the spatial patterns for the barystatic contribution to local sea level over the Arabian Sea and Bay of Bengal due to GRD and GIA.

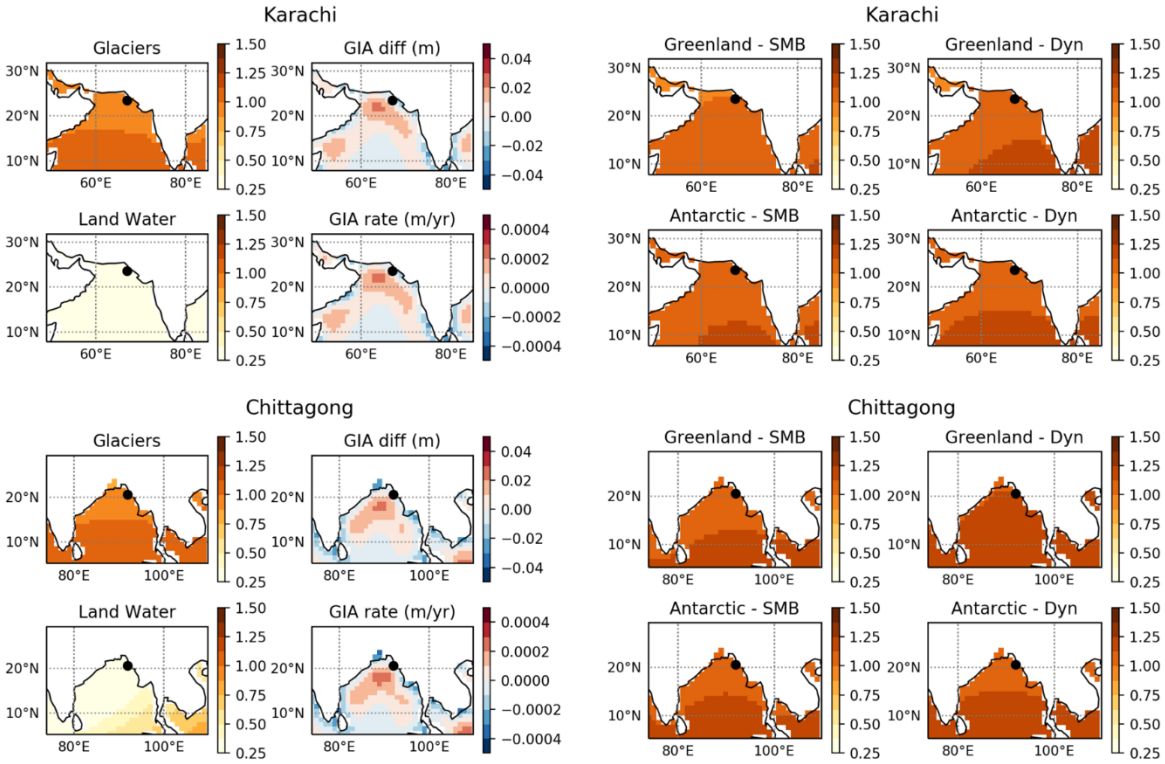

Figure A2.3: *Spatial patterns showing the contributions from global barystatic sea level changes to regional sea level change due to GRD, for the Arabian Sea (top row) and Bay of Bengal (lower row). These GRD estimates are expressed as local mean sea level per unit of global mean sea level change. The black circle indicates the location of representative tide gauge locations for each region. Karachi, Pakistan for the Arabian Sea and Chittagong, Bangladesh for the Bay of Bengal.*

The projections for local mean sea level changes at the South Asia tide gauge locations in this study, were derived from the Monte Carlo based GMSL projections, following the methods of UKCP18 (Palmer et al., 2018a)and (Palmer et al., 2020). The MSL projections are traceable to the same Monte Carlo procedure as the GMSL and preserve correlations between different components of sea level change (Palmer et al., 2018a). By retaining the information on correlations between sea level components, the contribution to the overall variance in local MSL change can be estimated for different combinations of the sea level components.

The four stages of the procedure for obtaining MSL projections from the Monte Carlo simulations are shown schematically in figure A2.4 and described further below:

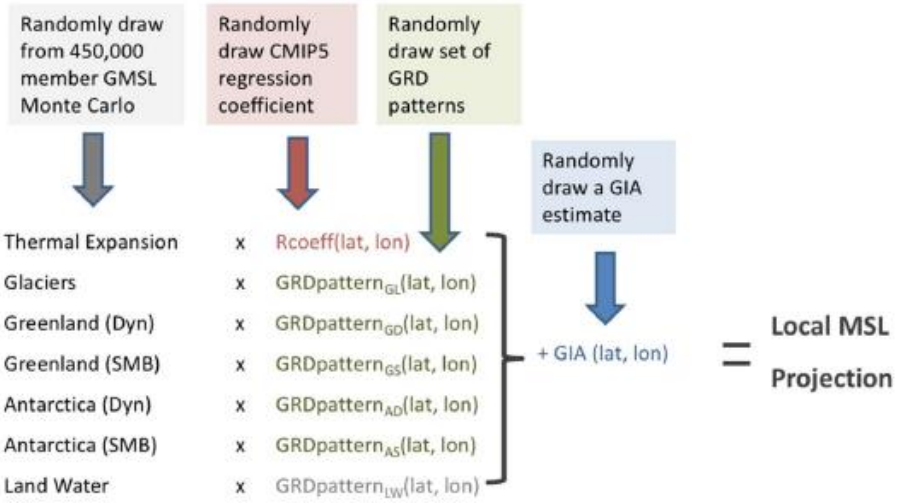

Figure A2.4: *Schematic representation of the Monte Carlo simulation performed for the South Asia regional mean sea level (MSL) projections. The above process is repeated 100,000 times to form a distribution of projected changes for each tide gauge location under each of the three RCP scenarios.*

1. Each instance of the 450,000-member Monte Carlo ensemble provides a set containing seven timeseries, with one timeseries for each of the seven components of GMSL. An instance is randomly drawn from the Monte Carlo ensemble, which provides timeseries for the seven components of GMSL.

2. Next, one of the available GRD models is randomly selected and the GRD spatial patterns are applied to timeseries for barystatic components of GMSL, providing timeseries for GRD contributions to MSL at the tide gauge locations. Except for the land water storage component, the GRD patterns all use the same (randomly selected) GRD model. For the land water storage component, the resulting GRD contributions to local MSL are based estimates from a single GRD solution (Slangen et al., 2014). The GRD estimates provide timeseries for six components of local MSL change.

3. For each tide gauge location, we determine regression coefficients for the changes in sterodynamic sea level per increment of thermosteric GMSL rise in each of the 21 CMIP5 models. The remaining timeseries for thermosteric sea level from Monte Carlo instance is combined with a regression coefficient randomly selected from the 21 CMIP5 models. This results in a timeseries for the estimated sterodynamic sea level change at each of the tide gauge locations.

4. The seven timeseries, corresponding to the six barystatic components and one sterodynamic component are combined with an estimate for the contribution due to GIA (section 2.4). The GIA estimated is provided by a random selection from one of the three GIA models. For each tide gauge location, the procedure is repeated 100,000 times to generate a distribution for projected MSL changes,

with each of the three RCP scenarios. As with IPCC AR5 GMSL projections, the spread is based on the 5th and 95th percentiles of the resulting distributions for the different components and for the combined MSL change.

A3 Sea level projections: extended discussion

A3.1 Contributions to global mean sea level projections

The GMSL projections for the 21st century show similar ranges to the GMSL projections presented in IPCC AR5 (Church et al., 2013) and projections from SROCC (Oppenheimer & Glavovic, 2019). The updated estimate for the contribution from Antarctica ice dynamics from Levermann et al. (2014) results in increases to the overall uncertainties and the skew of the distribution. For RCP8.5 the central estimate for GMSL rise is slightly higher compared the 21st century projections from IPCC AR5 and SROCC. The extended GMSL projections for the period 2100-2300 based on the 16 emulated CMIP5 models are consistent with the 21st century projections derived from the 21 CMIP5 models. The ranges for the overlapping period are within a few centimetres.

The extended projections highlight the long-term commitment to GMSL rise across the three RCP scenarios. The extended projections also highlight long-term differences between the scenarios, with larger differences between projections over the extended period when compared to the 21st century projections. In contrast the 21st century projections are broadly consistent across scenarios for first half of the century.

The contribution to GMSL rise from the melting of worldwide glaciers is restricted by the remaining glacier ice mass. In the extended projections the glacier component is capped at 0.32m, representing the total contribution to sea level rise following the melting of all estimated remaining glacier ice mass (Farinotti et al., 2019; Grinsted, 2013). Due to the tendency of temperature to increase the air moisture capacity, the removal of the remaining ice mass could occur later in scenarios with warmer surface temperature due to enhanced snowfall. For RCP4.5, the total remaining ice mass is depleted between 2100 and 2300. Under RCP8.5 the depletion of worldwide glacier ice mass occurs during 2200 and 2300. The extended GMSL projections are broadly consistent with the projections for 2300 presented in IPCC SROCC (Oppenheimer et al. 2019) with projected ranges of approximately 0.5-2.0 m and 2.0-5.0 m at 2300 for RCP2.6 and RCP8.5, respectively.

In the 21st century and 2300 projections, the contribution from the sea level components to overall uncertainty is assessed based on the 5th to 95th percentile range from the corresponding Monte Carlo distribution. The Antarctic components are the leading source of uncertainty for the 21st century and extended range projections, under all scenarios. Increased air temperatures over the Antarctic results in enhanced moisture transport due to increased moisture carrying capacity of the warmer air. The

associated increase in snowfall over Antarctica results in a net accumulation of ice-mass through deposition (positive mass balance), rather than a net loss of ice mass to the oceans through melting. The net accumulation of ice-mass from the Antarctic surface mass balance term can offset or exceed the ice-mass loss through Antarctic ice dynamics. Hence the 5th to 95th percentile range for combined Antarctica components includes negative values, where surface ice mass deposition (i.e. negative ice-mass loss) is the dominant process (Palmer et al., 2020). In general, the contributions and uncertainties for the components of GMSL (based on 5th to 95th percentile range) increase under higher forcing scenarios.

In the 21st century projections, there are large increases in the range of contributions from the Greenland ice sheet and the glacier mass changes. In the extended range projections under RCP8.5, the net contribution from the Antarctica components is negative for nearly the entire 5th to 50th percentile range. The eventual depletion of the remaining ice-mass stored in worldwide glaciers in the extended projections reduces the contribution to overall uncertainty from the glacier component. Hence, there is less uncertainty for RCP4.5 and RCP8.5, which result in complete depletion of worldwide glacier mass (see section 3.1).

The contributions from the separate components to overall uncertainty combine in a non-linear way, due to the underlying relationships (correlations) between the Monte Carlo timeseries for the different terms. The source of this non-linearity can be seen in the corresponding correlation matrix, based on the 5th to 95th percentile ranges in component timeseries from 450,000-member Monte Carlo ensemble. The thermosteric, glacier and Greenland surface mass balance components are positively correlated. There are enhanced contributions from these terms under a warmer climate. In contrast the Antarctica surface mass balance term is negatively correlated with these three terms, which results from the net ice-mass gain from the enhanced snowfall over the Antarctic in a warmer climate. For Antarctica the surface mass balance and ice dynamics components are weakly correlated. In contrast the corresponding Greenland components are generally uncorrelated.

A3.2 Regional Sea level changes

The projected changes for time mean sea level at the tide gauge locations in the Bay of Bengal region were compared with corresponding changes in global time mean sea level over the period 2006-2100 relative to 1986-2005, for RCP2.6, RCP4.5 and RCP8.5. There are clear geographical differences in projected sea level rise, that are common across RCPs, but these differences are small in magnitude. In general, the projected sea level rise at tide-gauge locations in the south of the region are slightly higher compared to the projected rise in global sea level. In contrast the projected sea level rise at tide-gauge locations in north of the region are slightly lower when compared with the projected rise in global sea level. The projected changes for tide-gauge locations in the west of the region are slightly smaller than for locations at similar latitude in the east of the region, meaning the largest increases are generally seen in

the northeast of the basin with the smallest increases in the southwest of the basin. The east-west differences are smaller compared to the north-south differences.

For example, for Port Blair located in the Andaman Islands (11.681 N, 92.767 E) at the far south east of the Bay of Bengal region, the projected changes are slightly larger than the projected global changes. For the period 2081-2100 under RCP2.6, projected local changes for the 5th, 50th and 95th percentiles represent 85%, 105% and 112% of the corresponding GMSL changes. While for RCP8.5 the changes at Port Blair represent 90-93% of the projected GMSL change. The scenario independent components (Antarctica ice dynamic, land water storage and glacial isostatic adjustment) are 0.38 cm lower for the midpoint contribution to local MSL relative to GMSL. The net contribution from the remaining scenario dependent components is 3.18 cm larger for local sea level under RCP2.6 and 2.34 cm larger for RCP8.5 compared to equivalent contributions to GMSL. The largest differences are seen between local sterodynamic sea level and global thermosteric sea level changes, with differences of 2.5 cm and 1.37 cm for RCP2.6 and RCP8.5 respectively. For Port Blair, Antarctica surface mass balance is the only scenario dependent component, for which the contribution to sea level change is lower than the contribution to global mean sea level change. The differences in the Antarctica surface mass balance contribution are small, around 0.1 cm and 0.2 cm for RCP2.6 and RCP8.5 respectively. In contrast, the projected changes in west of Bay of Bengal region for Nagapattinam (10.767 N, 79.850 E) are slightly lower compared to the projected global changes. Similarly, the projected changes at Chittagong (22.247 N, 91.875 E) and Diamond Harbour (22.200 N, 88.167 E) in the north of the Bay of Bengal region are lower compared to the projected global mean sea level rise over the same period.

The North-South differences between Chennai and Diamond Harbour under RCP2.6 range from 3.3 cm, 2.6 cm and 1.9 cm, while for RCP8.5 the differences are 2.5 cm, 3.0cm and 3.6 cm. The zonal difference in the Bay of Bengal are smaller, around 2.5 cm for RCP2.6 and 1.7 cm for RCP8.5. Sea level rise is larger in the east of the basin. The east west difference is lower under RCP8.5

For the Arabian Sea the projected changes are generally lower than projected changes to GMSL under both RCP2.6 and RCP8.5, except for locations in the far south of the region. Much of the difference between regional and global sea level change is determined by the spatial patterns arising from ocean mass change (GRD). Projected changes at Karachi are lower for projected changes to GMSL under both RCPs but the difference is smaller for RCP8.5 by approximately half. For RCP2.6 the sterodynamic contribution accounts for 55% of the central estimate for total sea level change, and 90% and 50% of the lower and upper bound estimates respectively. For comparison the thermosteric contribution to global sea level rise under RCP2.6 ranges from 35-40% of total projected GMSL change. Sterodynamic changes make a larger contribution to sea level rise in the north of the Arabian sea, compared to the global average. An increase in sterodynamic change (e.g. from ocean thermal expansion) would be expected to result in smaller difference between regional sea level rise and GMSL. For RCP8.5 the sterodynamic contribution accounts for 60 % of the central

estimate for total sea level change, just under 75% for the lower bound estimate and 50% for the upper bound estimate. The thermosteric contribution to GMSL accounts for around 40-45%. This suggests ocean thermal expansion and circulation changes will be the main driver of future sea level changes in the Arabian Sea. The uncertainty as indicated by the 5th to 95th percentile range is larger for sterodynamic change than for the other components, spanning around 0.1 at Karachi for RCP2.6 and 0.2m under both RCP4.5 and RCP8.5. The range for the sterodynamic contribution at given location is larger than differences between locations. For example, under both RCPs the projections at Cochin (India) exceed those at Karachi by around 0.05 m at both the lower, central and upper estimates. The West-East differences in the sterodynamic contribution are even smaller (on the order of millimetres).

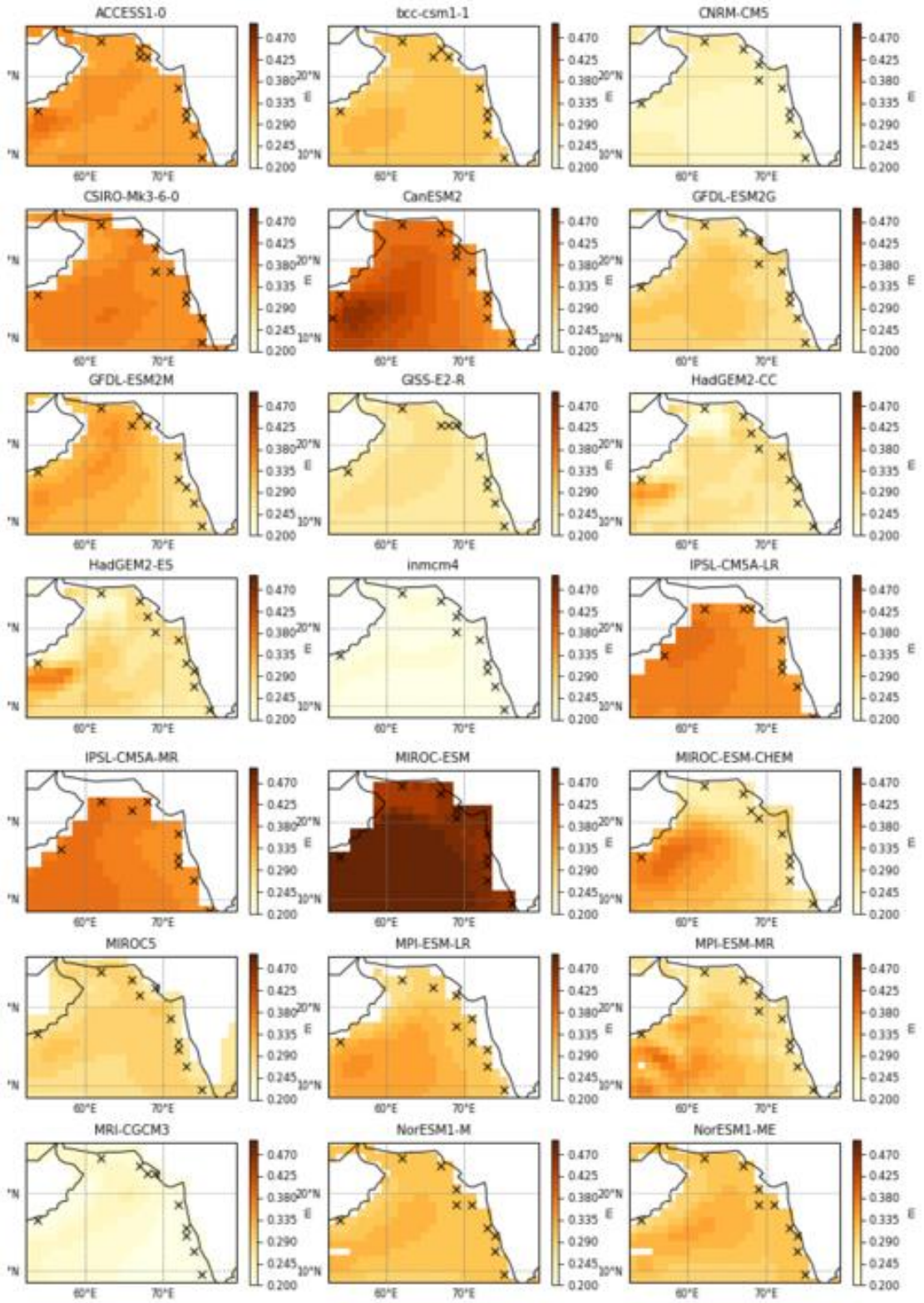

Figure A3.1: *Spatial patterns of sterodynamic sea level change over the Arabian Sea, region in each of the 21 CMIP5 models for the period 2081-2100 relative to 1981-2000. The label above each panel corresponds to the CMIP5 model used (see table A1 for model description). The black crosses indicate the model grid point used to represent the tide-gauge locations*

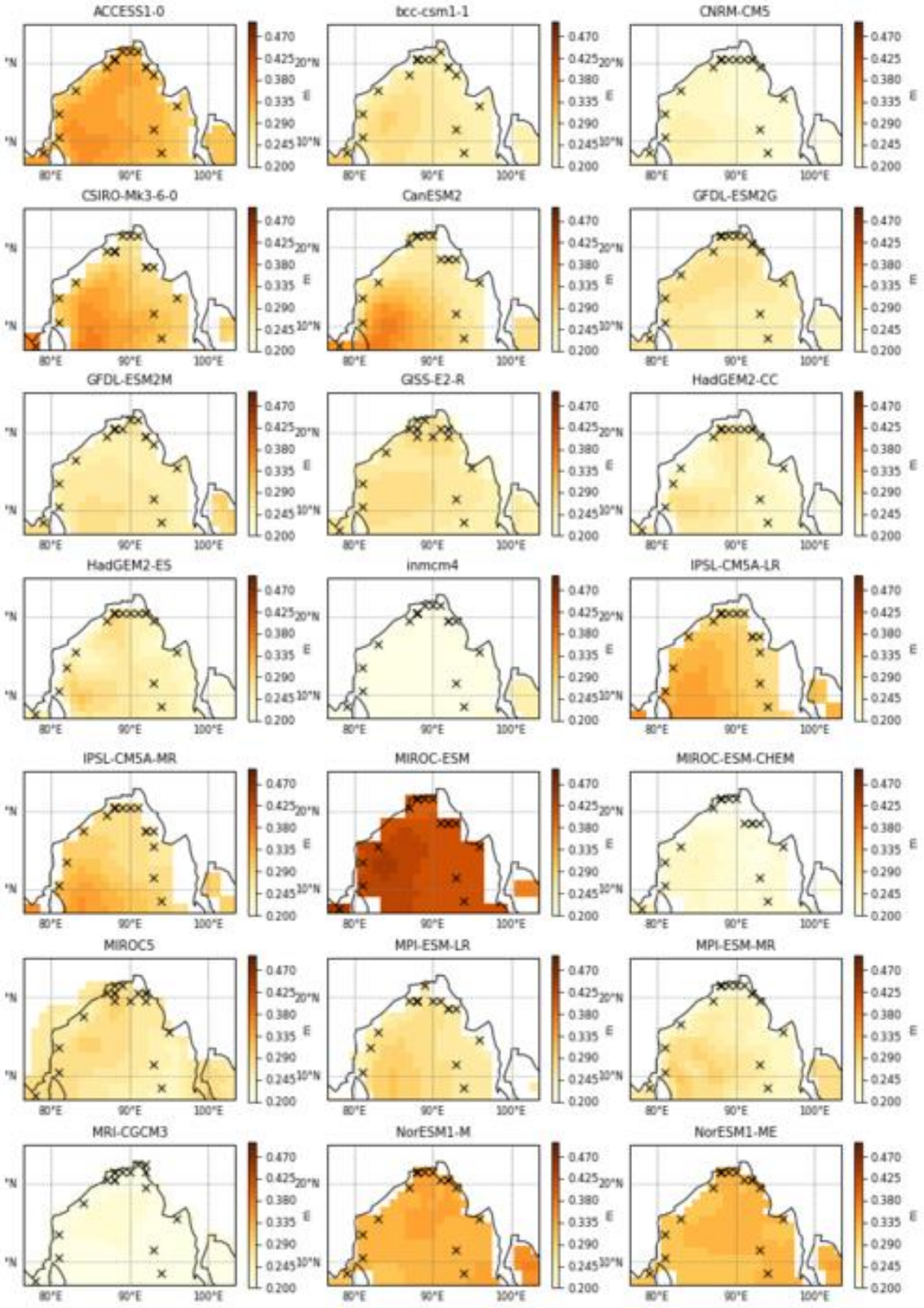

Figure A3.2: *Spatial patterns of sterodynamic sea level change over the Bay of Bengal regions in each of the 21 CMIP5 models for the period 2081-2100 relative to 1981-2000. The label above each panel corresponds to the CMIP5 model used (see table A1 for model description). The black crosses indicate the model grid point used to represent the tide-gauge locations*

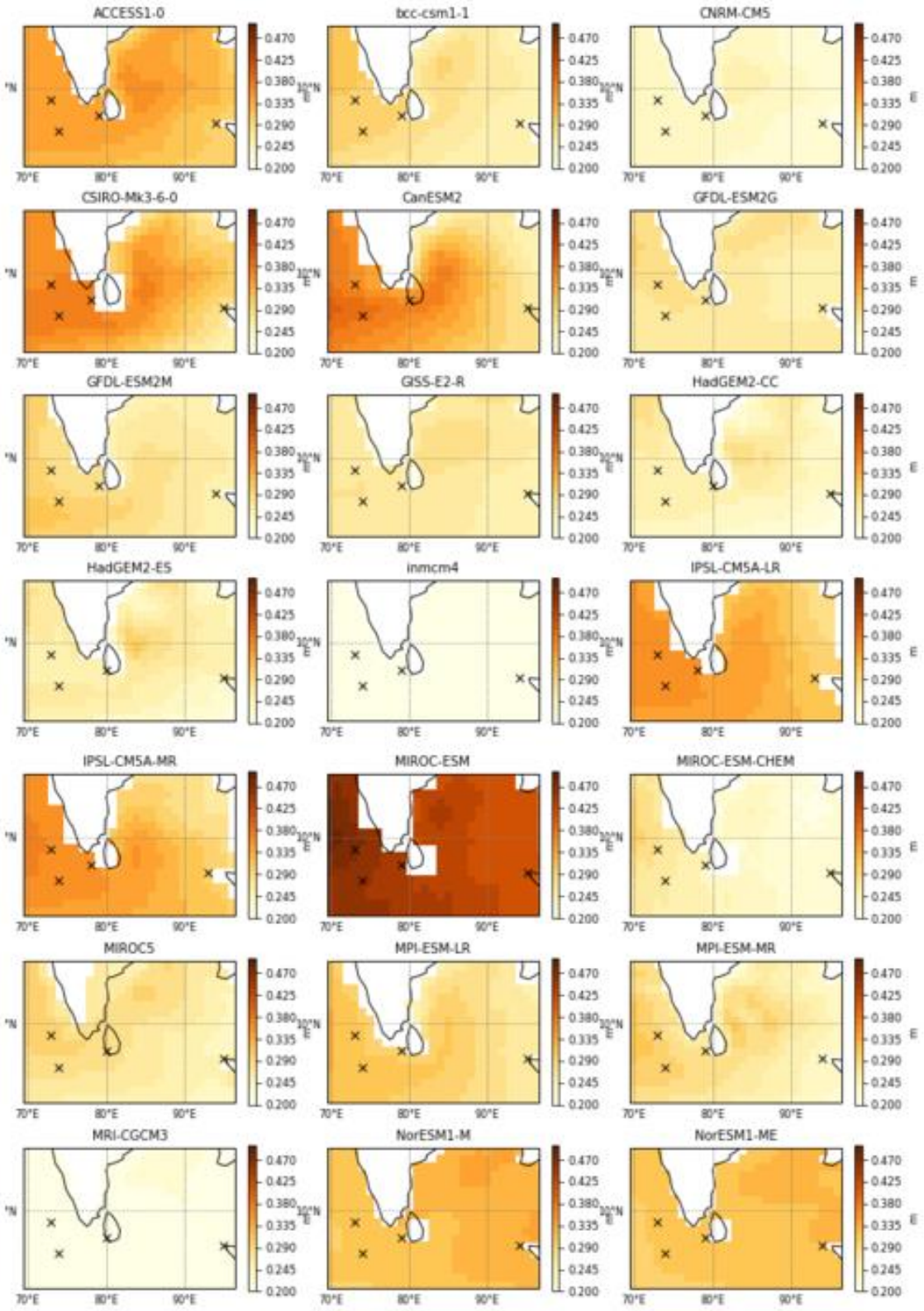

Figure A3.3: *Spatial patterns of sterodynamic sea level change over the Equatorial Indian Ocean region in each of the 21 CMIP5 models for the period 2081-2100 relative to 1981-2000. The label above each panel corresponds to the CMIP5 model used (see table A1 for model description). The black crosses indicate the model grid point used to represent the tide-gauge locations*.

References

Argus, D. F., Peltier, W. R., Drummond, R., & Moore, A. W. (2014). The Antarctica component of postglacial rebound model ICE-6G_C (VM5a) based on GPS positioning, exposure age dating of ice thicknesses, and relative sea level histories. *Geophysical Journal International*, *198*(1), 537–563. https://doi.org/10.1093/gji/ggu140

Cannaby, H., Palmer, M. D., Howard, T., Bricheno, L., Calvert, D., Krijnen, J., et al. (2016). Projected sea level rise and changes in extreme storm surge and wave events during the 21st century in the region of Singapore, *12*(3), 613–632. https://doi.org/10.5194/os-12-613-2016

Church, J. A. (2013). *IPCC AR5 Chapter 13: Sea Level Change Supplementary Material. In: Climate Change 2013: The Physical Science Basis. Contribution of Working Group I to the Fifth Assessment Report of the Intergovernmental Panel on Climate Change Coordinating Lead Authors: L*. *IPCC AR5*. Jan H. van Angelen.

Church, J. A., P.U. Clark, A. Cazenave., J.M. Gregory., S. Jevrejeva., A. Levermann., et al. (2013). *Change 2013: The Physical Science Basis. Contribution of Working Group I to the Fifth Assessment Report of the Intergovernmental Panel on Climate Change* . *Jan Lenaerts*. Jan H. van Angelen.

DeConto, R. M., & Pollard, D. (2016). Contribution of Antarctica to past and future sea-level rise. *Nature*, *531*(7596), 591–597. https://doi.org/10.1038/nature17145

Edwards, T. L., Brandon, M. A., Durand, G., Edwards, N. R., Golledge, N. R., Holden, P. B., et al. (2019). Revisiting Antarctic ice loss due to marine ice-cliff instability. *Nature*, *566*(7742), 58–64. https://doi.org/10.1038/s41586-019-0901-4

Farinotti, D., Huss, M., Fürst, J. J., Landmann, J., Machguth, H., Maussion, F., & Pandit, A. (2019). A consensus estimate for the ice thickness distribution of all glaciers on Earth. *Nature Geoscience*, *12*(3), 168–173. https://doi.org/10.1038/s41561-019-0300-3

Gregory, J. M., Griffies, S. M., Hughes, C. W., Lowe, J. A., Church, J. A., Fukimori, I., et al. Concepts and Terminology for Sea Level: Mean, Variability and Change, Both Local and Global, 40 Surveys in Geophysics § (2019). Springer Netherlands. https://doi.org/10.1007/s10712-019-09525-z

Grinsted, A. (2013). An estimate of global glacier volume. *The Cryosphere*, *7*(1), 141–151. https://doi.org/10.5194/tc-7-141-2013

Gupta, A. Sen, Jourdain, N. C., Brown, J. N., & Monselesan, D. (2013). Climate Drift in the CMIP5 Models. *Journal of Climate*, *26*(21), 8597–8615. https://doi.org/10.1175/JCLI-D-12-00521.1

Holgate, S. J., Matthews, A., Woodworth, P. L., Rickards, L. J., Tamisiea, M. E., Bradshaw, E., et al. (2012). New Data Systems and Products at the Permanent Service for Mean Sea Level. *Journal of Coastal Research*, *29*(3), 493–504. https://doi.org/10.2112/JCOASTRES-D-12-00175.1

Legeais, J.-F., Ablain, M., Zawadzki, L., Zuo, H., Johannessen, J. A., Scharffenberg, M. G., et al. (2018). An improved and homogeneous altimeter sea level record from the ESA Climate Change Initiative. *Earth System Science Data*, *10*(1), 281–301. https://doi.org/10.5194/essd-10-281-2018

Levermann, A., Winkelmann, R., Nowicki, S., Fastook, J. L., Frieler, K., Greve, R., et al. (2014). Projecting Antarctic ice discharge using response functions from SeaRISE ice-sheet models, *5*(2), 271–293. https://doi.org/10.5194/esd-5-271-2014

Mitrovica, J. X., Tamisiea, M. E., Davis, J. L., & Milne, G. A. (2001). Recent mass balance of polar ice sheets inferred from patterns of global sea-level change. *Nature*, *409*(6823), 1026–1029. https://doi.org/10.1038/35059054

Oppenheimer, M., & Glavovic, B. (2019). Chapter 4: Sea Level Rise and Implications for Low Lying Islands, Coasts and Communities. IPCC SR Ocean and Cryosphere. *IPCC Special Report on the Ocean and Cryosphere in a Changing Climate [H.- O. Pörtner, D.C. Roberts, V. Masson-Delmotte, P. Zhai, M. Tignor, E. Poloczanska, K. Mintenbeck, M. Nicolai, A. Okem, J. Petzold, B. Rama, N. Weyer (Eds.)]. In Press.*, *Chapter 4*(Final Draft), 1–14. https://doi.org/10.1126/science.aam6284

Palmer, M., Howard, T., Tinker, J., Lowe, J., Bricheno, L., Calvert, D., et al. (2018). *UKCP18 Marine Report*. Retrieved from www.metoffice.gov.ukwww.metoffice.gov.uk

Palmer, M. D., Gregory, J. M., Bagge, M., Calvert, D., Hagedoorn, J. M., Howard, T., et al. (2020). Exploring the Drivers of Global and Local Sea-Level Change over the 21st Century and Beyond. *Earth's Future*. Retrieved from https://onlinelibrary.wiley.com/doi/abs/10.1029/2019EF001413

Peltier, W. R. (2004). GLOBAL GLACIAL ISOSTASY AND THE SURFACE OF THE ICE-AGE EARTH: The ICE-5G (VM2) Model and GRACE. *Annual Review of Earth and Planetary Sciences*, *32*(1), 111–149. https://doi.org/10.1146/annurev.earth.32.082503.144359

Peltier, W. R., Argus, D. F., & Drummond, R. (2015). Space geodesy constrains ice age terminal deglaciation: The global ICE-6G_C (VM5a) model. *Journal of Geophysical Research: Solid Earth*, *120*(1), 450–487. https://doi.org/10.1002/2014JB011176

Slangen, A. B. A., Carson, M., Katsman, C. A., van de Wal, R. S. W., Köhl, A., Vermeersen, L. L. A., & Stammer, D. (2014). Projecting twenty-first century regional sea-level changes. *Climatic Change*, *124*(1–2), 317–332. https://doi.org/10.1007/s10584-014-1080-9

Spada, G., & Stocchi, P. (2007). SELEN: A Fortran 90 program for solving the "sea-level equation." *Computers and Geosciences*, *33*(4), 538–562. https://doi.org/10.1016/j.cageo.2006.08.006

Wada, Y., van Beek, L. P. H., Sperna Weiland, F. C., Chao, B. F., Wu, Y.-H., & Bierkens, M. F. P. (2012). Past and future contribution of global groundwater depletion to sea-level rise. *Geophysical Research Letters*, *39*(9), n/a-n/a. https://doi.org/10.1029/2012GL051230